

INVASIVE SPECIES SPREAD MAPPING USING MULTI-RESOLUTION REMOTE SENSING DATA

Le Wang

Dept. of Geography, Assistant Professor, University at Buffalo, the State University of New York, 105 Wilkeson Quad., Buffalo, NY 14261, lewang@buffalo.edu

KEY WORDS: Classification, Saltcedar, Spectral Unmixing

ABSTRACT:

The invasions of non-native species of vegetation pose significant threats to natural environments at all geographical scales. Saltcedar has been commonly treated as one of the several most threatening invasive species in U.S. in the next ten years. The spatial extent and density of infestation by saltcedar in the Rio Grande floodplain has been poorly understood in the past. Remote sensing provides a unique tool to map and monitor invasive species and provides a mean to detect major land cover changes and quantify the rate of change. To date, remote sensing has been mainly applied for mapping some canopy dominant invasive species. Accurate mapping of saltcedar distribution and abundance in a timely manner plays a central role to assist the undertaking of an effective control. Current studies have largely concentrated on the large-area detection with coarse resolution remote sensing data. Nevertheless, it is lacking of studies that systematically evaluate the respective potential of high spatial resolution satellite imagery, airborne hyperspectral imagery, as well as moderate resolution imagery for mapping saltcedar's extents, distribution and monitoring its spread over time. Such cost and benefit analysis will be particularly invaluable to the regional or national scale study, in which selection of an appropriate image type to maximize the outcome plays an important part. In this study, a comprehensive test was designed and carried out to examine the ability to integrate multi-temporal and multi-resolution imagery: including very-high spatial resolution (QuickBird), hyperspectral resolution imagery (AISA), and moderate resolution satellite imagery (Landsat TM), in differentiating saltcedar from other riparian vegetation types in the Rio Grande river basin. Two types of analyses were fulfilled: first, five pixel-based classification methods were adopted for assessing effectiveness of QuickBird and AISA, respectively, i.e., the Maximum Likelihood Classifier (MLC), Neural Network Classifier (NNC), Support Vector Machine (SVM), Spectral Angle Mapper (SAM), and Maximum Matching Feature (MMF); Second, Landsat TM imagery was synthesized from AISA and tested for mapping abundance of saltcedar with four linear spectral unmixing methods and three back-propagation neural network methods. Results indicated that AISA outperformed QuickBird imagery in differentiating saltcedar from other riparian vegetation species. SVM achieves the highest classification accuracy among all the five classifiers. Linear spectral unmixing method exhibited similar mapping accuracy with neural network methods in estimating abundance of saltcedar at a spatial resolution of 30 by 30 square meters, but with significantly better computing efficiency. Overall, this study reflects the maximum capability of contemporary remote sensing in assisting reconnaissance of saltcedar, the most threatening invasive species in southwest United States.

1. INTRODUCTION

Since 1837, eight species of *Tamarix* (family Tamaricaceae) have been introduced into the U.S. from Europe, Asia, and Africa for ornamentals, windbreaks, and erosion prevention of stream banks (Baum, 1967). In the arid and semiarid southwestern United States, three common naturalized *Tamarix* species are: *T. parviflora*, *T. chinensis*, and *T. ramosissima*. Given the fact that variations among the three species are not constant and hardly to be discerned even in the field, saltcedar has been used to as a universal name to refer to all the three species in most ecological studies. Saltcedar has extensively invaded riparian sites and quickly assumed dominance in the southwestern U.S. and northern Mexico with its superior capability to tolerate drought and produce high leaf area as well as high density stands (Cleverly et al. 1997). In the Rio Grande basin, where was recently identified as the most vulnerable site to saltcedar in the nation (Morissette, JT et al. 2006), saltcedar has deteriorated the existing water shortage problem as it consumes more water than the native vegetation it replaced. Estimates on water consumption by saltcedar and associated species vary greatly depending on location, maturity, density, and depth of groundwater. An accurate method is therefore urgently needed to take inventory of such noxious plants, allowing the identification of location, density, and mass of invasive species in comparison to native species. The efficient control of such dynamic non-native species also demands timely discovery and continuous monitoring of their spread.

Remote sensing provides a unique tool to map and monitor invasive species and provides a mean to detect major land cover changes and quantify the rate of change. To date, remote sensing has been applied for mapping and modeling some of canopy dominant invasive species with imagery acquired at different spatial and spectral resolution. Since 1999, high-spatial resolution data become available from commercial satellite such as IKONOS and Quickbird. Both IKONOS and Quickbird sensors have been used for detecting giant reed and spiny aster in southern Texas (Everitt and Yang, 2004), and detect malaleuca trees (*Malaleuca quinquinervia*) in south Florida (Fuller, 2005). In the later, the author reported that IKONOS was limited in detecting small stands of scattered seed trees, which would be necessary in the predictive models. High spatial resolution satellite image has the merit of repetitive coverage of a large spatial area with low costs. However, the efficacy of such imagery in saltcedar mapping has not yet been fully investigated.

Compared to the multi-spectral remote sensing data, hyperspectral sensors are capable of capturing much finer spectral information reflected off the plant, and thus, adding in power to the species discriminations. To date, several invasive species have been successfully detected with hyperspectral sensors including iceplant (*Carpobrotus edulis*), jubata grass (*Cortaderia jubata*) (Underwood et al., 2003), leafy spurge (O'Neill, 2000; William and Hunt, 2002; Glenn et al., 2005), Brazilian pepper (Lass and Prather, 2004), spotted knapweed and babysbreth (Lass et al. 2005). However, as far as saltcedar was

concerned, it is surprising to note that no study has been conducted by using hyperspectral remote sensing data. Such fact may result from two reasons. First, there are fewer hyperspectral sensors that can be chosen from compared to its counterpart with the multispectral sensor. Among the limited hyperspectral sensors, EO-1 is the only viable space-borne sensor. But given its coarse spatial resolution (30 meter), low signal-to-noise ratio as well as the inflexibility for scheduling the flyover, it may be suitable for assessing the saltcedar abundance within a 30 meter square, but not possible to derive the species level saltcedar information. Whereas, airborne hyperspectral sensors, among which AVIRIS, CASI and AISA are the three mostly popular ones, can provide hyperspectral information at very fine spatial resolution ranging from 1 meter to 4 meters. The accrued spectral and spatial resolution may suffice the task to map species-level saltcedar information. Nevertheless, to apply airborne hyperspectral sensors in wide geographical regions is cumbersome given the limited coverage by the airborne sensor and high cost incurred in the acquisition process.

If the entire lower Rio Grande region, which journeyed through several hundreds of miles, is to be tasked for assessing spatial spread of saltcedar, imagery like QuickBird or AISA, will not suffice a feasible solution due to enormous costs. At this scale, moderate resolution satellite imagery, such as Landsat TM, is an ideal source of input given its wide spatial coverage and low acquisition costs. Recent advancements in sub-pixel mapping from Landsat TM have allowed quantifying sub-pixel percentage (abundance) of species coverage. The underlying rationale to correspond species abundance to sub-pixel mapping is that mixed pixels from remote sensing are resulted from a systematic combination of component spectra (end-members) present in the sensor's instantaneous Field of view (IFOV) (Adams et al., 1993). The relative contribution of component spectra is then determined by the inversion of mixture models. Previously, Landsat TM/ETM+, has been found useful for mapping large dense patches of weeds, but when applied to small stands, these methods have limited capability for weed detection.

In short, saltcedar has been commonly treated as one of the several most threatening invasive species in U.S. in the next ten years (saltcedar consortium). Accurate mapping of its distribution and abundance in a timely manner play a pivotal role to assist the undertaking of an effective control. Currently, it is lacking of studies that systematically evaluate the respective potential of the emerging high spatial resolution, hyperspectral resolution imagery, and moderate resolution imagery in reconnaissance of saltcedar distribution as well as monitoring its temporal spread. Such cost-and-benefit analysis will be particularly invaluable to the regional or national scale study in which selection of an appropriate image type to maximize the outcome plays an important part. To this end, the objectives in this study are two-fold: 1) Comparing classification performance of QuickBird and Hyperspectral AISA sensor. Through the comparison, We aim to derive a general conclusion of the merit and drawback of the aforementioned two types of remote sensing images in species-level saltcedar mapping; 2) Comparing four Linear Spectral Unmixing (LSU) methods and three neural networks methods for mapping sub-pixel abundance of saltcedar and associated native species with Landsat TM imagery.

2. STUDY SITES AND DATA PREPARATION

2.1 Study sites

The study site is located in the middle Rio Grande River, near the town of Candelaria, TX (Figure 1). Canyons and small valleys

comprise the physical geography of this stretch. The climate in this region is arid and semi-arid, with average annual precipitation less than 10 inches (most of which falls during the summer growing season), and average temperatures around 90°F. The majority of the lands bordering this stretch are private ranches and rangeland, with some residential land. The vegetation on both banks of the river is composed of mostly saltcedar (*Tamarix Chinensis* L.) with some mixes of willow (*Salix* spp). As one moves into the uplands, the honey mesquite (*Prosopis* spp) is found, although it is generally mixed with other bushes, weeds and saltcedar. A giant saltcedar species (*Tamarix aphylla* (L.) Karst, also athel tamarisk) is also present in this study site, although in very sparse occurrences along the uplands. The athel tamarisk is an evergreen tree of up to 12 meters in height when mature with not overlapping (strongly clasping) leaves.

2.2 Data preparation

One scene of Spaceborne Quickbird image was acquired on Dec. 8, 2004. This image covers an area of 5-by-10 kilometers centered at 30.12°N latitude and 104.69°W longitude. The image was radiometric- and geometrically calibrated using the standard remote sensing package ENVI v4.1 (Research System Inc. 2004). In order to take advantage of both the multispectral and panchromatic bands, a pansharpening process was run to produce multispectral bands with the maximum allowed spatial resolution (0.61m). The image, when delivered by the vendor, is already in geo-referenced format. However, further registration was carried out through ground control points collected on site with GPS units delivering data at sub-meter accuracy.

The acquisition of a hyperspectral AISA image was carried out on Dec 23, 2005. The Airborne Imaging Spectroradiometer for Applications (AISA) sensor system was calibrated to measure 62 bands of spectral information in the range of 430 to 1000 nm at the spatial resolution of 1m. Because the swath of the sensor is much narrower than that of QuickBird's, five strips of images were mosaiced to cover the entire area. The AISA mosaic was co-registered with the QuickBird's pan sharpened image.

One Landsat TM image (only bands 1-4) was synthesized from QuickBird owing to the fact that the spectral characteristics of QuickBird and Landsat ETM+ sensors at bands 1-4 are comparable. Therefore, no further spectral re-sampling was required, but only spatial re-sampling. The synthesized Landsat TM image was produced by aggregating the pixels of each QuickBird image. Disjoint windows of 12-by-12 pixels were used, resulting in a spatial resolution of 28.8m, which approximates that of landsat sensors.

Two field trips (Nov. 17-19, 2004, Dec.17-19, 2005) were arranged to collect sufficient ground truthing data in the study sites. GPS polygon samples were drawn along dense patches of several species located in the area. The second field campaign was concurrent with the AISA image acquisition. Hyperspectral measurements were taken using a portable hand-held spectro-radiometer (ASD VNIR Field Spectrometer). These measurements are useful for image spectral analysis and calibration.

Based on our field observations, a detailed classification system was designed (Table 1). This classification system is meant to cover the most important species and land cover types found in the study site. Splitting of saltcedar in three Categories was necessary in order to avoid misclassification errors due to phenology variability.

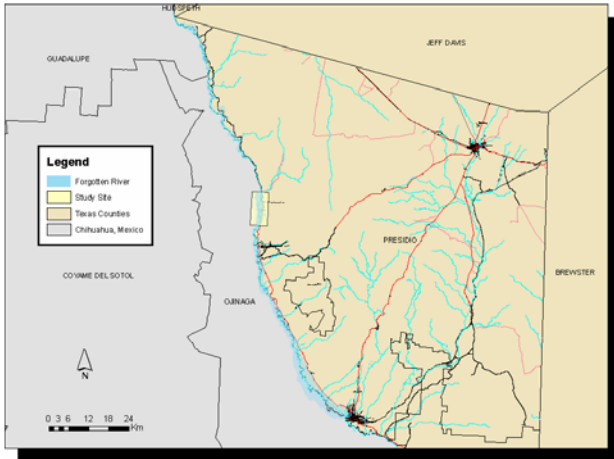


Figure 1. Geographic location of the study site

	Class Title	Description
1	Saltcedar - green-brown	Areas mainly covered by saltcedar (<i>Tamarix Chinensis</i>) with predominantly green leaves; it may have some dry branches.
2	Saltcedar - orange-brown	Areas mainly covered by dry saltcedar (<i>Tamarix Chinensis</i>) prior to its dormant phenological stage
3	Giant saltcedar	Areas mainly covered by giant saltcedar (<i>Tamarix aphylla</i>) with green leaves
4	Mesquite	Areas mainly covered by honey mesquite trees (<i>Prosopis glandulosa</i>)
6	Poverty weed	Areas mainly covered by poverty weed (<i>Iva axillaris Pursh</i>)
7	Marsh weed	Areas mainly covered by marshy weed (<i>Limmophila</i>), with possible occurrences of Gooddings's willow
8	Creosote bush	Areas mainly covered by creosote bush (<i>Larrea tridentata</i>), characterized by its sparse distribution on the hilly areas
5	Mysterious bush	Unknown bushes, usually in small stands
9	Herbaceous - green	Areas mainly covered by green herbaceous plants and grasses
10	Herbaceous - dry	Areas mainly covered by dry herbaceous plants and grasses
11	Wetland	Emergent herbaceous wetlands, as well as other irregularly inundated areas that may not be vegetated
12	Water	Either shallow or deep water bodies
13	Road	Asphalt paved road
14	Gravel	Areas predominantly covered by barren gravel, including gravel roads
15	Roof	House's roof of any kind
16	Sand	Areas predominantly covered by sandy bare ground

Table 1. Land cover classes used in the classification of the study site

3. METHODOLOGY

3.1. Band Selection

Selecting appropriate bands is an important step that leads to successful classification. This is particularly true for classification of hyperspectral imagery. In this study, different band combinations were devised and tested for QuickBird and AISA (Table 2). Band selection for Quickbird consists of both the original and pan-sharpened multispectral bands. Pan-sharpened bands were produced using the Gram-Schmidt spectral sharpening tool built in ENVI system (v4.2). The pan-sharpened image was co-registered and wrapped to the AISA imagery to end up with 1m resolution image. Additionally, QuickBird multispectral bands were synthesized from AISA. Synthesis of QuickBird was carried out using the ENVI's spectral resampling tool with predefined QuickBird filter functions; then, pixels were spatially aggregated to match the QuickBird resolution (2.4m). The synthesized QuickBird were incorporated in this test with an aim to remove possible atmospheric and phenological factors that could have influenced the performance of 2004 QuickBird data.

Band selection for the ASIA sensor was done in several ways. The first way uses all the 61 narrow bands in the VNIR region. The second way uses only four bands: band 11 (481.39nm), band 20 (563.17nm), band 30 (656.99) and band 46 (823.25), which have wavelength centers that coincide with those of Quickbird imagery (485, 560, 660 and 830nm, respectively). The third band selection strategy is based on results from a linear discriminant analysis (LDA). The objective of LDA is to determine the optimal bands, computed as linear combinations from the original bands that maximize the linear separability of the training data. Since many of the relative weights, used to compute each new band (LDA band), are small with respect to the maximum weight, they can be set to zero. Thus, multiplications and additions can be saved for the non-contributing bands. In our case, we set zero for all the weights falling below half of the maximum weight for each LDA band. A fourth band selection strategy is through the minimum noise fraction (MNF) transform. The MNF transform, like the principal component analysis (PCA), is used to determine the intrinsic dimensionality of the data. However, unlike PCA, the MNF is not orthogonal. The axes of the MNF transform are aligned along the axis of minimum noise fraction (maximum signal to noise ratio), rather than along the principal components (directions of maximum variance).

3.2. Image classification for QuickBird and AISA

Five pixel-based methods were tested in this research. They are: Maximum Likelihood Classifier (MLC), Neural Network classifier (NN), Support Vector Machine (SVM), Spectral Angle Mapper (SAM), and Maximum Matching Feature (MMF).

The MLC method maximizes the posterior probability that a pixel site is covered with a land cover class, given the observed spectral information of the pixel (Richards and Jia 1999). The final output of the MLC method is the class that has the largest

Sensor	Band Selection	Classification	
		Method	Method ID
QuickBird	4 multispectral bands	MLC	MLC_QB
QuickBird	4 multispectral bands	NNC	NNC_QB
QuickBird	4 multispectral bands	SVM	SVM_QB
QuickBird	4 pansharpened (1m)	MLC	MLC_PAN_QB
AISA	4 QuickBird synth.	MLC	MLC_AISA2QB
AISA	4 narrow bands	MLC	MLC_AISA4
AISA	4 narrow bands	NNC	NNC_AISA4
AISA	61 bands	SAM	SAM_AISA61
AISA	61 bands	MMF	MMF_AISA61
AISA	7 LDA bands	MLC	MLC_LDA7_AISA
AISA	7 LDA bands	SVM	SVM_LDA7_AISA
AISA	10 MNF bands	MLC	MLC_MNF10_AISA
AISA	10 MNF bands	SVM	SVM_MNF10_AISA

Table 2. Different band combinations and classifiers

probability. For this method to be operable, an assumption is made that all the classes have a multivariate Gaussian distribution defined in the feature space. This assumption simplifies the classification problem, to the point where only the mean vector and the covariance matrix are required for each class. The performance of the MLC method is generally acceptable for multispectral data sets where the number of bands is usually below ten. For large number of bands, this method turns

impractical, as it requires a great number of training samples for the estimation of the covariance matrix.

The SAM method represents an alternative when dealing with large number of bands (Kruse et al.1993). In this case, the spectral information of each pixel is considered as a vector of dimensions equal to the number of bands. The geometrical concept of angle between vectors is then extended to such higher dimensional space. The SAM method uses the (spectral) angle as a similarity measure to classify every pixel. The logic of this method is similar to that of a minimum distance classifier, where the class having the minimum distance to (or highest similarity with) an end-member is selected. An end-member is a single vector (or spectral signature) that is representative of the class; for example, the average of the training data. The advantages of SAM method are 1) it can operate with large number of bands, 2) it is insensitive to scaling of the spectral values, caused by changes in the illumination. The major limitations are that: 1) the angle has no physical interpretation, and 2) it treats all the classes in the same way, e.g., having same variability.

The use of NN method is generally suggested when the discriminating surfaces in the feature space are too complex, or when the Gaussian assumption is violated (Benediktsson et al. 1990, Kavzoglu and Mather 2003). This occurs, for example, when two or more categories having different spectral signature are aggregated in a single class. NNC are network structures composed of basic processing elements called neurons, usually arranged in layers. In isolation, neuron units perform linear combinations of the input and compares the result by differencing with a threshold (also called activation level). The residual from the comparison is evaluated through a transfer function (also called activation function) that has the shape of a sharp step. The result is then a binary value that can be interpreted as: the input belongs (high output), or does not belong (low output) to a class. Weight and threshold parameters are adjusted by a process known as training. In practice, since most training methods are based on gradient search strategy, they require derivable transfer functions, such as the sigmoid function. The NNC used here was a feed forward network with two hidden layers. The network was trained in MATLAB system (v6.5.1) using a resilient back-propagation (RBP) algorithm. The RBP learning rule uses gradient direction, without the magnitude, to adjust the weight parameters using a fixed learning rate. This method was selected because it trains faster than traditional gradient descent methods and works generally well with categorical values.

SVM is a classification method derived from statistical learning theory. It was originally designed for binary classification, but can function as a multiclass classifier by combining several binary classifiers (Wu et al. 2004). Each binary SVM classifier separates two classes with a decision surface that maximizes the margin between the classes. The surface is often called the optimal hyperplane, and the data points closest to the hyperplane are called support vectors. The support vectors are the critical elements of the training set, as they alone define (support) the optimal hyperplane. If the two classes are non-linearly separable, the method uses a kernel function to map the data to a higher dimension where the data is linearly separable. The hyperplane found in the higher dimensional space results in a complex non-linear boundary when projected back a lower dimensional space. As with neural networks, the processing of large datasets through SVM method requires a lot of computation time. Here we used the implementation available in ENVI 4.3 System, which provides a hierarchical, reduced-resolution classification

process that improves performance without significantly degrading results.

The MMF selects the class that has maximum abundance derived using the so-called matched filtering (MF) technique (Boardman et al. 1995). MF finds the abundances of user-defined end-members using a partial unmixing. Unlike full linear unmixing techniques, MF is not restricted to the knowledge of all end-members in the image. This technique maximizes the response of the known end-member and suppresses the response of the composite unknown background, thus matching the known signature. It provides a rapid means of detecting specific materials based on matches to library or image end-member spectra and does not require knowledge of all the end-members within an image scene.

3.3. End-member selection

In this study, three end-members were devised: Invasive species, Native species and Clear. Spectral reflectance for each end-member was derived from the training data collected in the field and AISA image. The end-members are plotted in figure 2. This figure shows the location of end-member on the plane spanned by the two principal components, which explain 99.6% of the total variance. It also shows the two-dimensional histogram of mixed pixels (background image) and points from a set of signatures for sixteen land-cover classes laid out in table 1 (labeled crosses). These signatures were selected from the original AISA imagery with the aid of GPS points acquired in the field. The signatures were re-sampled to match the TM spectral characteristic and then projected onto the PCA plane. Each land-cover type in table 1 was assigned to one of the three categories used (as indicated by the color): Invasive (red), Native (green) and Clear (blue). The two-dimensional plot reflects the major data distribution, thus revealing that the end-member for the Invasive category is interior to the cloud of mixed pixels.

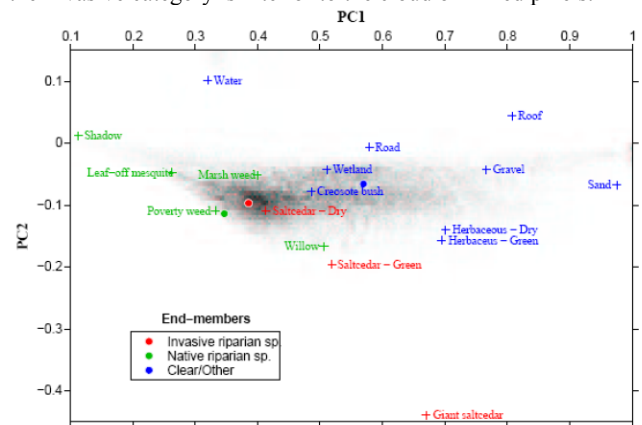


Figure 2: Location of image end-members and land cover spectra on the plane spanned by the two principal components.

3.4. Species abundance mapping with linear and non-linear spectral unmixing

Four LSU and three NN mixture models were adopted to derive sub-pixel abundance of saltcedar. The general LSU mixture model is expressed in Equation (1):

$$y = X\alpha + \epsilon \quad (1)$$

Where the matrix X is formed by three end-members, y stand for the observed mixed pixels, α is the abundance or land cover fractions to be estimated, and ϵ represents residual that is not explained by the three end-members.

Given end-members and mixed pixels are known, equation (1) can be solved using four formulations: first, unconstrained least square solution as introduced by Ravishanker (2002); second, classical constrained least square that considers the ‘sum-to-one’ constraint (Heinz and Chang, 2001; Hu et al., 1999), termed in this paper as SCLSU; Third, a ‘non-negativity’ constrained LSU, termed as NCLSU (Chang and Heinz, 2000); Last, a fully constrained (both ‘sum-to-one’ and ‘non-negativity’) least square LSU (Heinz and Chang, 2001), termed as FCLSU.

A BPNN is a multi-layered feed-forward neural network trained by the so-called back-propagation algorithm (Rumelhart et al., 1986). This learning algorithm is an iterative gradient descent training procedure. The network weights are first randomly initialized. Then, the input data are presented to the network and propagated forward to estimate the output value for each training example. The difference (error) between known and estimated outputs is minimized by updating the weights in the direction of the descent gradient. The process is repeated, with weights being recalculated at each iteration until the error is minimal or lower than a given threshold. For the unmixing problem, the BPNN associates spectral signatures to land cover fractions by learning from training sets. After training, the neural network system fixes all the weights and maintains the original learning parameters. Then, a similar process takes place in which fractions are predicted from image pixels using the parameters learned from the training set. It has to be noted within this setting, the network cannot explain how mixed pixels are related to end-members. Before training a BPNN, many design parameters need to be selected either experimentally or from previous experience. These parameters include the number of hidden layers, neurons per layer, number of training iterations, etc. In this study, three BPNN were trained with one hidden layer of 5, 10 and 20 neurons, respectively (hereafter referred to as BPNN5, BPNN10 and BPNN20). One input node per band (four inputs) and one output neuron per class (two outputs) were employed. Only the classes Invasive and Native are predicted by the network, whereas the class Clear is determined from the sum-to-one condition. Each neuron computes a log-sigmoid function of the weighted sum of its input. The updates of the weights and activation level parameters were carried out using the resilient back-propagation optimization method (trainrp, Riedmiller and Braun, 1993), with early stop strategy for better generalization behavior. The early stop criterion prevents over-fitting of the training data by monitoring the errors committed on independent validation data. The early stopping is controlled by the number of time the validation performance increased since the last time it decreased (max fail). This parameter was set to 20. Another stopping criterion is controlled by the number of iterations (epochs). This parameter was set to 1500.

4. RESULTS AND DISCUSSION

4.1 Classification performance of QuickBird

The results for the QuickBird image are summarized in Table 3. The user and producer accuracies correspond to the aggregated class consisting of the three saltcedar classes in Table 1. Three classifiers: MLC, NNC, and SVM performed very similarly, yet MLC achieved the highest overall accuracy. Given its simplicity, the MLC method was selected for testing the incorporation of the panchromatic band. The results indicate inclusion of panchromatic band does not improve classification accuracy, instead, it tends to enlarge the spectral confusion, resulting in lower user and producer accuracies. The MLC method was also applied to the synthetic QuickBird image. The results indicate

that the atmospheric effects play a significant role in the classification accuracy of the acquired QuickBird. Specifically, the overall accuracy from the synthetic image increased more than 10% with respect to the acquired QuickBird.

Method	Overall	Kappa	Producer	User
	Accuracy	Statistics	Accuracy*	Accuracy*
MLC_QB	70.9	0.69	77.7	71.8
NNC_QB	66.9	0.65	69.3	69.3
SVM_QB	70.2	0.68	70.3	79.5
MLC_PAN_QB	70.6	0.68	72.5	68.3
MLC_AISA2QB	82.0	0.81	89.6	93.9

Table 3. Classification accuracies for QuickBird (accuracies for saltcedar categories only)

4.2. Classification performance of AISA

The results for the AISA image are summarized in Table 4. Since the AISA image contains more detailed spectral information, higher overall and individual classification accuracies were expected. However, results indicate that the processing of hyperspectral data has to be done with much care. Those methods that use all the hyperspectral bands (SAM and MMF) performed poorer, when compared with the results from QuickBird. Band selection generally increased the performance, even in the case of the selection of the four narrow bands aligned with the QuickBird band-pass filters. The best band selection method was the MNF. The SVM gave the highest accuracy when the MNF band selection was adopted. Yet, the MLC performed very close to SVM. A reason for this may be due to the fact that all the classes defined in this study does not exhibit complex spectral variability. In fact, the spectral variability of saltcedar was largely avoided by differentiating three sub-classes: Saltcedar green-brown, Saltcedar orange-brown and Giant saltcedar (evergreen), which present distinct spectral characteristics.

Method	Overall	Kappa	Producer	User
	Accuracy	Statistics	Accuracy*	Accuracy*
SAM_AISA61	68.6	0.66	84.8	94.7
MMF_AISA61	45.0	0.42	45.8	78.6
MLC_AISA4	84.5	0.83	89.4	91.4
NNC_AISA4	63.9	0.62	95.1	87.1
SVM_AISA4	86.6	0.86	92.7	94.9
MLC_LDA7_AISA	86.6	0.86	92.7	94.9
SVM_LDA7_AISA	85.8	0.85	91.9	94.8
MLC_MNF10_AISA	87.6	0.87	93.7	94.6
SVM_MNF10_AISA	87.7	0.87	93.9	96.5

Table 4. Classification accuracies (* Accuracies from saltcedar categories only)

Table 5 shows the weights (after weight thresholding and vector normalization) of the optimal linear transformation derived from LDA. Each LDA band is responsible for discrimination of two or more land cover classes. In particular, band LDA3 is responsible for discriminating most of the apparent Saltcedar. This can be observed by visual correlation of the known saltcedar stands with the values in LDA3. Not surprisingly, the most significant AISA bands used for computing the LDA3 band fall in the visible range, specifically in the green and orange regions of the visible spectrum. The band LDA3 band can be interpreted as the difference between two slopes. The first slope occurs in the

region 520-545nm (near the green edge) and the other in the region 600-640nm (near the orange edge). These two regions are associated with the green vegetation reflectance peak and red absorption peak.

4.3.LSU results

Table 6 presents the RMSE performance of four LSU methods for predicting reflectance and sub-pixel area. These results show that all LSU models can predict accurately the reflectance of mixed pixels (with standard errors under 1% in most cases). However, none of them can lead to accurate sub-pixel area estimation. Even the best performed methods (FCLSU, TLSU and NCLSU) can lead to errors that are in the order of 28% the pixel size. This means that small fractions could not be accurately mapped with none of these LSU methods. In summary, the abundances derived from FCLSU are the most accurate, followed by TLSU and NCLSU. .

Method	RMSE*	
	Reflectance [%]	Area [m ²]
UCLSU	0.1247	14.8635
NCLSU	0.3910	8.5349
SCLSU	0.6305	19.5734
FCLSU	1.6603	8.2487
TLSU	0.3167	8.5024

* Results based on the pooled test sets.
Table 6 Results of four LSU methods

4.4.Comparison of BPNN and LUS results

Among three BPNN methods, BPNN5 performed the best. A comparison was then made between the best performed LSU method (FCLSU) and the best performed BPNN method (BPNN5). Tables 7(a) and (b) present the sub-pixel confusion matrices, a new sub-pixel assessment tool proposed by Silvan and Wang (2008). The most significant difference between the matrices is noted at the intersection of the first and second rows with the first column. BPNN5 presents higher agreement for Invasive class (79.2%) than FCLSU (59.5%). This is also portrayed in the user and producer accuracies shown in Table 7(c). Note the higher difference in producer accuracies from FCLSU with respect to producer accuracies from BPNN5. A marginal improvement of around 2% was obtained from BPNN5, as given by the overall accuracy (OA). The number of parameters and computer time required by each classifier are presented in Tables 7(d). The CPU time required for the training and testing were measured in MATLAB. The processing used a laptop SONY VAIO with Pentium 4 CPU running at 2.8GHz and 512MB of RAM memory. The training time for FCLSU consists of the computation time of the end-members, which was negligible since training data was available, whereas the training time for the BPNN5 was around 8 seconds. In contrast, FCLSU required much more time than BPNN5, in nearly a factor of sixty.

5. CONCLUSIONS

In order to examine the potential of contemporary remote sensing in mapping saltcedar at different spatial scales, a comprehensive study was conducted using multi-resolution multi-source remote sensing imagery encompassing QuickBird, AISA, and Landsat TM. Results indicated that AISA hyperspectral imagery

outperformed QuickBird imagery in differentiating saltcedar from other riparian vegetation species. SVM achieves the highest classification accuracy among all the five adopted classifiers. Linear spectral unmixing method exhibited similar mapping accuracy with neural network methods in estimating abundance of saltcedar at a spatial resolution of 30 by 30 square meters, but with significantly better computing efficiency, one important factor that has to be taken account in order to tackle regional scale saltcedar spread from remote sensing. Overall, this study investigates almost the best capability of contemporary remote sensing in assisting reconnaissance of saltcedar, the most threatening invasive species in southwest United States.

AISA Band	WL [nm]	LDA1	LDA2	LDA3	LDA4	LDA4	LDA6	LDA7
8	454.27						0.3039	
9	463.31						0.3694	
11	481.39						0.2967	
12	490.42	0.3366						
14	508.50	-0.3406			0.3148			
15	517.54			-0.3251			-0.4695	
16	526.58						-0.5193	
17	535.61						-0.3364	
18	544.67			0.4081				
19	553.89				-0.3318		0.2827	-0.4489
21	572.45	0.5569	0.4744		0.4365			
22	581.78				0.3525	-0.4277		0.4989
23	591.18			-0.5623				
24	600.58	-0.5106	-0.7204	-0.3604				
25	609.98	-0.447						
26	619.39			0.3176	-0.5435			
27	628.79				-0.2837			
29	647.59					0.5915		-0.7413
31	666.39			0.4252				
32	675.80					0.515		
33	685.20				0.3163			
35	704.02						-0.4494	
36	713.45		0.5059					

Table 5. coefficients for the optimal linear transformation from LDA. Blanks represent zeroes.

Class	Reference (%)			Total
	Inva	Nati	Clear	
Inva	59.5	11.3	15.9	26.9
Nati	27.3	80.4	11.1	37.6
Clear	13.2	8.2	73.0	35.4
Total	100.0	100.0	100.0	100.0

a

Class	Reference (%)			Total
	Inva	Nati	Clear	
Inva	79.2	16.8	19.8	36.8
Nati	12.3	74.2	10.3	32.3
Clear	8.6	9.0	69.9	35.0
Total	100.0	100.0	100.0	100.0

b

Class	FCLSU		BPNN5	
	Prod. Acc.	User Acc.	Prod. Acc.	User Acc.
Invasive	59.5	63.3	79.2	62.2
Native	80.4	67.5	74.2	75.6
Clear	73.0	82.0	69.9	84.4

OA = 71.51 ($\kappa = 0.5704$) OA = 73.84 ($\kappa = 0.6079$)

c

Method	Parameters	Time [ms]	
		Train (300)	Test (600)
FCLSU	12	0	1756
BPNN5	37	7718	30

d

Table 7 Comparison of LSU and BPNN (a) Sub-pixel confusion matrix for FCLSU; (b) Sub-pixel confusion matrix for BPNN5; (c) Accuracy indices for each method; (d) Computation cost

REFERENCES

Adams, J. B., Smith, M. O., Gillespie, A. R. 1993. Imaging spectroscopy: Interpretation based on spectral mixture analysis. In Remote Geochemical Analysis: Elemental and Mineralogical Composition, C. M. Pieters and P. Englert, Eds. Cambridge Univ. Press (1993), pp. 145-166.

Baum, B.R. 1967. Introduced and naturalized tamarisks in the United States and Canada [Tamaricaceae].

Baileya 15:19-25 Benediktsson, J. A., Swain, P. H. and Ersoy, O. K., 1990, Neural network approaches versus statistical-methods in classification of multisource remote-sensing data. IEEE Transactions on Geoscience and Remote Sensing, 4, 540-552.

Boardman, J. W., Kruse, F. A., and Green, R. O., 1995, Mapping target signatures via partial unmixing of AVIRIS data: in Summaries, Fifth JPL Airborne Earth Science Workshop, JPL Publication 95-1, v. 1, pp. 23-26.

Chang, C.-I, Heinz, D. C., 2000. Constrained sub-pixel target detection of remotely sensed imagery. IEEE transaction on Geoscience and Remote Sensing 38 (3), 1114-1159.

Cleverly, J. R., Smith, S. D., Sala, A. and Devitt, D. A. 1997. Invasive capacity of Tamarix ramosissima in a Mojave Desert floodplain: the role of drought. Oecologia 111,12-18.

Everitt, J.H., Yang, C., Davis, M.R. 2004. Remote mapping of two invasive weeds in the Rio Grande system of Texas. American Water Resources Association Conference Proceedings.

Fuller, D.O., 2005. "Remote detection of invasive Malameuca trees (Malaleuca quinquenervia) in South Florida with multispectral IKONOS imagery". Int. Journal of Remote Sensing 26(5):1057-1063.

Glenn, N.F., J.T. Mundt, K.T. Weber, T.S. Prather, L.W. Lass, J. Pettingill. 2005. "Hyperspectral data processing for repeat detection of small infestations of leafy spurge". Remote Sensing of Environment 95:399-412.

Heinz, D. C., Chang, C.-I, 2001. Fully constrained least square linear spectral unmixing analysis method for material quantification in hyperspectral imagery. IEEE Transactions on Geoscience and Remote Sensing 39 (3), 529-545.

Hu, Y. H., Lee, H. B., Scarpace, F. L., 1999. Optimal linear spectral unmixing. IEEE Transactions on Geoscience and Remote Sensing 37 (1), 639-644.

Kavzoglu, T., Prather, P. M., 2003, The use of backpropagation artificial neural networks in land cover classification. Int. J. Remote Sensing, 24 (23), 4907-4938.

Kruse, F. A., Lefkoff, A. B., Boardman, J. B., Heidebrecht, K. B., Shapiro, A. T., Barloon, P. J., Goetz, A. F. H., 1993, The Spectral Image Processing System (SIPS) - Interactive Visualization and Analysis of Imaging spectrometer Data. Remote Sensing of Environment, 44, 145 - 163.

Lass, L.W., and T.S. Prather, 2004. "Detecting the locations of Brazilian pepper trees in the Everglades with hyperspectral sensor". Weed Technology 18:437-442.

Lass, L.W., T.S. Prather, N.F. Glenn, K.T. Weber, J.T. Mundt, J. Pettingill. 2005. "A review of remote sensing of invasive weeds and example of early detection of spotted knapweed (Centaurea maculosa) and babysbreath (Gypsophila paniculata) with a hyperspectral sensor". Weed Science 53:242-251.

Morissette, J. T., Jarnevich, C. S., Ullah, A., Cai, W., Pedelty, J. A., Gentle, J. E., Stohlgren, T. J., and Schnase, J. L., 2006. A tamarisk habitat suitability map for the continental United States. Front Ecol Environ 4(1):11-17.

O'Neill, M., Ustin, S. L., Hager, S., Root, R. (2000). Mapping the distribution of leafy spurge at Theodore Roosevelt National Park using AVIRIS. In: Proc. Ninth JPL Airborne Visible Infrared Imaging Spectrometer (AVIRIS) Workshop, Jet Propulsion Laboratory, Pasadena, CA.

Ravishanker, N., Dey, D., 2002. A first course in linear model theory. Boca Raton: Chapman and Hall/CRC, xvi, 473 p.

Richards, J. A., Jia, X., 1999. Remote Sensing Digital Image Analysis (3rd Edition). Berlin: Springer-Verlag.

Rumelhart, D. E., Hinton, G. E., Williams, R. J., 1986, Learning representations by back-propagating errors. Nature 323, 533-536.

Silvan J., L. Wang. 2008. Sub-pixel confusion-uncertainty matrix for assessing soft classifications, Remote Sensing of Environment, in press.

William, P.A. and E.R. Hunt. 2002. "Estimation of leafy spurge cover from hyperspectralimagery using mixture tuned matched filtering". Remote Sensing of Environment. 82:446-456.

Wu, T.-F., C.-J. Lin, and R. C. Weng., 2004, Probability estimates for multi-class classification by pairwise coupling. Journal of Machine Learning Research, 5, 975-1005.

Underwood, E., S. Ustin, D. DiPietro, 2003. "Mapping non native plants using hyperspectralimagery" Remote Sensing of Environment 86:150-161

ACKNOWLEDGEMENTS

The study was supported by grants to L. Wang from US Department of Agriculture CSREES Award # 2004-38899-02181, and US Geological Survey via Texas Remote Sensing Consortium. Thanks should go to Mr. Jose Silvan for helping with computer programming and field data collection and analysis.